*Geol. Mag.* **145** (*5*), *2008, pp. 685–701. © 2008 Cambridge University Press*
doi:10.1017/S0016756808004901 *Printed in the United Kingdom*


# The Euphrates volcanic field, northeastern Syria: petrogenesis of Cenozoic basanites and alkali basalts

NANCY A. LEASE & ABDEL-FATTAH M. ABDEL-RAHMAN*

Ministère de l'Agriculture, des Pêcheries et de l'Alimentation, 200 chemin Sainte-Foy, Québec (Québec), G1R 4X6, Canada, and Department of Geology, American University of Beirut, P.O. Box 11-0236, Beirut, Lebanon

(*Received* 16 March 2007; *accepted* 2 August 2007; First published online 29 April 2008)

**Abstract –** The Plio-Quaternary Euphrates volcanic field of NE Syria includes large discontinuous exposures of basanitic and basaltic lava flows (1200 $km^2$ in area). It represents the northern segment of the Cenozoic volcanic province of the Middle East and is located near the Bitlis collision suture. The rocks consist of olivine (15–20 %), clinopyroxene (30–35 %), plagioclase (45–55 %) and opaque phases. Chemically, the rocks are largely ultrabasic ($SiO_2$ 38.2–45.5 wt %, MgO 8.7–13.0 wt % and average Mg number of 0.65). They are enriched in incompatible trace elements such as Zr (133–276 ppm), Nb (25–71 ppm) and Y (17–28 ppm). The REE patterns are strongly fractionated ($(La/Yb)_N$ = 19.6), indicative of a garnet-bearing source. The $^{143}Nd/^{144}Nd$ isotopic compositions range from 0.512868 to 0.512940 ($\varepsilon_{Nd} = 4.5$ to 5.9), and $^{87}Sr/^{86}Sr$ from 0.70309 to 0.70352. These chemical and isotopic compositions reflect strong affinities to OIB. Elemental ratios such as K/P (3.4), La/Ta (13) and La/Nb (0.77), and the low $SiO_2$ values, suggest that the Euphrates magma was subjected to minimal crustal contamination. Petrogenetic modelling has been carried out using a variety of mantle source materials, different degrees of partial melting (0.1 to 10 %), and a number of scenarios including metasomatized sources. Modelling suggests that the magma could have been produced as a result of a small degree of partial melting of either (1) a garnet-bearing depleted source enriched with a small addition of metasomatizing fluids, or (2) a garnet-bearing fertile source. The overall chemical and petrological characteristics are more consistent with the generation of the Euphrates magma by a small degree of partial melting (F = 1 %) of a primitive, garnet-lherzolite mantle source, possibly containing a minor spinel component. The Neogene collision of the Arabian plate with Eurasia along the Bitlis suture resulted in reactivation (beneath the Euphrates basin) of deep-seated fractures, along which lavas may have penetrated the crust.

Keywords: basanite, northeastern Syria, olivine, Nd–Sr isotopes, petrogenesis, Euphrates graben, Bitlis suture.

## 1. Introduction

The Euphrates volcanic field is located in northeastern Syria near its borders with Iraq and Turkey. The volcanic field occurs at a tectonically active region and represents the northern segment of the Middle East Cenozoic volcanic province (Fig. 1). This province consists of large, discontinuous volcanic exposures extending from Sinai, Jordan and Israel, to Lebanon, Syria and Turkey (Dubertret, 1955; Mouty *et al.* 1992; Shaw *et al.* 2003; Abdel-Rahman & Nassar, 2004; Weinstein *et al.* 2006; Lustrino & Sharkov, 2006). Cenozoic volcanism has produced some other extensive volcanic provinces, although of very different styles, further south in east Africa (mostly Kenya and Ethiopia), in Yemen and in Arabia (Mohr, 1983; White & McKenzie, 1989; Camp & Roobol, 1992; Camp, Roobol & Hooper, 1992; Baker, Thirlwall & Menzies, 1996; Volker *et al.* 1997; Bertrand *et al.* 2003; Furman *et al.* 2004, 2006).

The Quaternary mafic lavas of northern Kenya were interpreted by Furman *et al.* (2004) as being derived from mixtures of plume and ambient mantle sources. Furman *et al.* (2006) demonstrated that the Tertiary mafic lavas of Kenya reflect isotopically distinct plume heads beneath Tanzania and Afar that are derived from the chemically heterogeneous South African superplume. In Ethiopia, the Cenozoic lava flows were interpreted to have been developed in association with the Afar plume (Barberi *et al.* 1975; Mohr, 1983; Hart *et al.* 1989; Stewart & Rogers, 1996; Barrat *et al.* 1998; Pik *et al.* 1999; George & Rogers, 2002), and are clearly related to the East African rift system. According to Ebinger & Sleep (1998), Cenozoic magmatism throughout east Africa resulted from impact of a single plume.

Baker, Thirlwall & Menzies (1996) demonstrated that the Oligocene flood basalts of western Yemen are also Afar plume products like those of similar age in Ethiopia. The Plio-Quaternary mafic lavas of western Yemen were interpreted to have been produced in response to small amounts of lithospheric extension that were metasomatized and hydrated by the Afar plume (Baker *et al.* 1997, 1998). Several comprehensive studies were carried out on the Cenozoic continental flood basalts of Saudi Arabia (e.g. Camp & Roobol, 1989, 1992; Camp, Roobol & Hooper, 1992). These

*Author for correspondence: arahman@aub.edu.lb

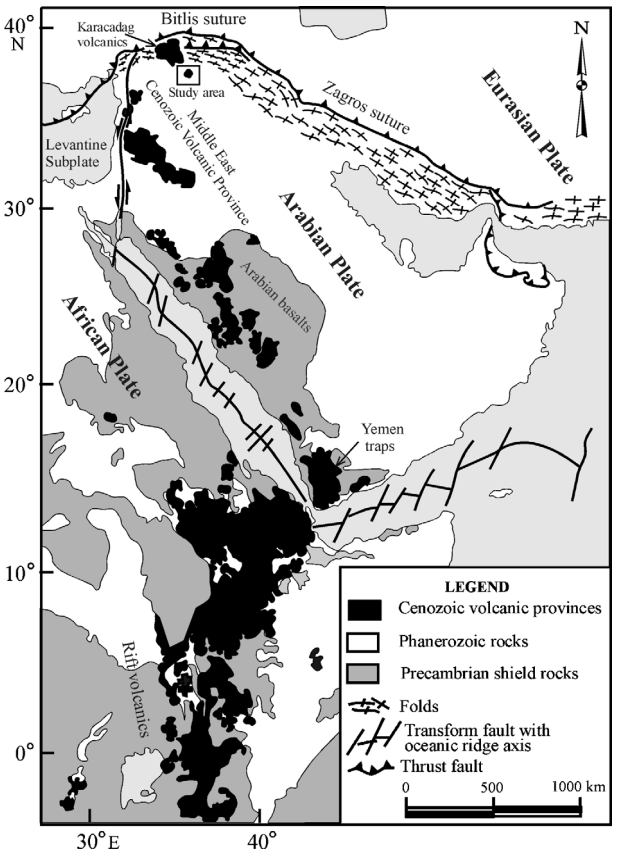


Figure 1. Regional geological map showing the distribution of the various Cenozoic volcanic provinces in east Africa, Arabia and the Middle East.

were interpreted to have occurred in two distinct phases. Phase one (30 to 20 Ma) of tholeiitic to transitional lavas was related to passive-mantle upwelling during extension of the Red Sea basin, and phase two (12 Ma to Recent) that produced transitional to strongly alkalic lavas was related to active-mantle upwelling facilitated by minor continental extension (Camp & Roobol, 1992). According to White & McKenzie (1989) and Camp & Roobol (1992), the source of upwelling is either a mantle plume centrally located beneath the West Arabian Swell, or an elongated and extended lobe of hot asthenosphere emanating from the Ethiopian mantle plume.

In sharp contrast, the Afar plume of Ethiopia is thought not to have been channelled northwestwards beneath the Arabian plate, and it has played no role in producing the Cenozoic volcanic field of Jordan (Shaw *et al.* 2003). These Jordanian alkali basalts and basanites were formed in response to a phase of lithospheric extension. Miocene basaltic magmatism in Sinai is interpreted by Baldridge *et al.* (1991) to have been related to the opening of the Red Sea. Garfunkel (1989) described the 'Cover' Cenozoic basalts, which are located in southeastern Galilee and in southern Golan heights, as mostly alkaline basalts of intraplate character and ocean-island basalt affinities and proposed that the Jordan Valley depression could have acted as a route for magma ascent. According to Weinstein *et al.* (2006), basanites and alkali basalts of the southern Golan and Galilee region have two mantle sources (a dehydrated garnet-bearing amphibole peridotite, and amphibole-garnet-bearing pyroxinite veins) occurring at lithospheric depths, and were formed by dehydration and partial melting of an originally isotopically uniform reservoir. Abdel-Rahman & Nassar (2004) interpreted the Pliocene alkali basalts of northern Lebanon to have erupted during an episode of localized extension, which occurred particularly at the junction between the Dead Sea–Ghab transform (Fig. 2a, b) and the Yammouneh restraining bend (that is, in a transtensional tectonic regime).

In their general study that included Cenozoic volcanism in Syria, Mouty *et al.* (1992) presented preliminary geochemical data and produced whole-rock K–Ar ages ranging from 23.5 to 1.5 Ma. They demonstrated that there was a large gap (between 16 and 8 Ma) in Cenozoic volcanic activity, and interpreted this to correspond with the interval between the two stages of spreading of the Red Sea–Dead Sea rift system. Mouty *et al.* (1992) further proposed that the rocks are mostly within-plate transitional to alkaline basalts, and that magmatism was associated with left-lateral movements along the Dead Sea rift. In their study of the Neogene alkaline mafic lavas of western Syria, Lustrino & Sharkov (2006) indicated that much of the volcanic activity in that region is concentrated near the Dead Sea transform fault system. They concluded that the origin of the lavas of western Syria reflects a strong lithospheric control on the loci of partial melting which developed as a result of mantle decompression formed as a consequence of the transition from strongly compressive to transtensional stresses, and that there is no evidence to relate volcanic activity to northwestward channelling of the Afar plume or to any other mantle plume.

Near the Bitlis suture zone, a large crustal segment (the Karacadağ volcanic plateau of southern Turkey; Fig. 2b), occurring to the north of the investigated volcanic field, is covered largely by Late Cenozoic lavas. K/Ar ages reported in Pearce *et al.* (1990), and Notsu *et al.* (1995) on these transitional to alkaline mafic lavas range from Upper Pliocene to Recent. Pearce *et al.* (1990) proposed that the lavas of southern Turkey were derived from the mantle lithosphere of the Arabian continent which had been enriched by small volumes of asthenospheric melts.

No modern petrological–geochemical data on the northeastern Syrian Cenozoic basalts are available in the published international literature, and their magma source and petrogenesis are far from certain. The aim of our study is as follows: (1) to provide petrological, chemical and isotopic data on the Euphrates volcanic field of Syria, (2) to characterize its mantle source and propose a petrogenetic model for its magma generation, and (3) to evaluate the tectonic regime of magma emplacement in the context of the geodynamic framework and nearby plate boundaries.

https://doi.org/10.1017/S0016756808004901 Published online by Cambridge University Press

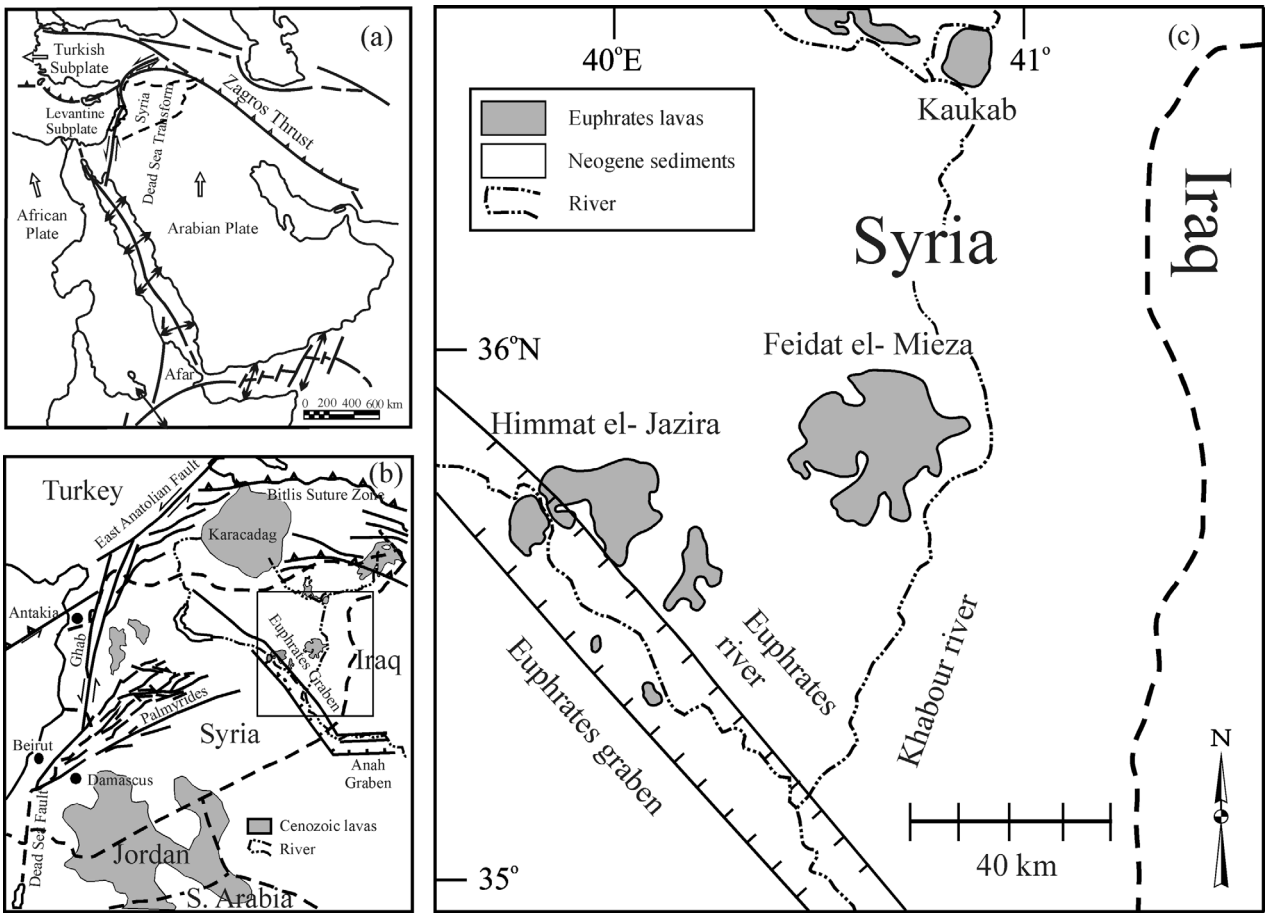


Figure 2. (a) Map showing the main tectonic elements in the Middle East. (b) Map showing the area of study and some of the structural elements. Area of small box is enlarged in (c). (c) Simplified geological map of northeastern Syria showing locations of the various exposures within the Euphrates volcanic field (after Ponikarov, 1967).

## 2. Geological setting

The Euphrates volcanic field of northeastern Syria is located between latitudes 35°00′ and 36°30′ N and longitudes 39°30′ and 41°00′ E (Fig. 2c). It occurs on the northern flank of the Arabian plate, and is situated near major plate boundaries and tectonically active regions (Fig. 2a, b). The Bitlis suture, the left-lateral East Anatolian fault, and the Zagros fold belt occur to the north and east of the investigated volcanic field. The left-lateral Dead Sea–Ghab transform fault system, located further to the west of the volcanic field, has been active since the end of the Miocene (Lyberis *et al.* 1992), and permits the northward movement of the Arabian plate and its collision with Eurasia along the Bitlis suture, occurring just to the north of the Euphrates volcanic field (Fig. 2a, b).

The Euphrates graben/fault system was developed by extension/transtension following a period of extensive uplift and erosion during the Jurassic and Early Cretaceous (A. Koopman, unpub. Syrian Petroleum Company Report, 1986; Sawaf *et al.* 1993). Litak *et al.* (1997) interpreted the reactivation of deep-seated fractures beneath the Euphrates graben to have resulted as a consequence of Neogene collision of the Arabian plate with Eurasia along the Bitlis suture. The presence of such an extensional graben near this collisional zone could also be interpreted to reflect the 'escape' of Turkey along the Anatolian fault system.

According to Giannerini *et al.* (1988), a change in plate motion occurred during Plio-Quaternary times, when the Arabian plate rotated to the northeast. This resulted in a transversal tension along the Levantine fault, with the Palmyrian fold belt behaving like a sinistral, intracontinental-transform fault. It should be noted that the Euphrates volcanic field occurs near the intersection between the Euphrates graben/fault system and the northeastern extension of the Palmyride fold zone. The various volcanic exposures lie in direct continuation of the Palmyride structural zone (Fig. 2b).

Lava flows of the Euphrates volcanic field overlie undeformed Neogene and Quaternary deposits; few old sedimentary sections are exposed in the region. Regional mapping of Dubertret (1955) showed the Neogene and Quaternary volcanic rocks of Syria and Lebanon to be fissure-type eruptions. He stated that lava ascended along re-activated as well as Recent fault planes, forming voluminous flows. Ponikarov (1967) also studied the general geology of Syria, which included the area under investigation.

https://doi.org/10.1017/S0016756808004901 Published online by Cambridge University Press

The Euphrates volcanic field includes the Ein Abou-Jema locality, which covers an area of about 30 km$^2$ of mafic–ultramafic lava flows, Himmat el-Jazira (400 km$^2$), Feidat el-Mieza (680 km$^2$) and Kaukab (100 km$^2$). These consist of lava flows and minor pyroclastic flows of Middle and Upper Quaternary age, overlying Neogene sediments. The lavas are mainly composed of phyric varieties (olivine basalts), forming fine-grained massive rocks with variable degrees of vesicularity. The flows form plateaux typical of shield-type volcanoes, and the lower unit in some of the volcanic piles is topped by craters with lava flows and associated pyroclastic materials, reflecting mixed effusive and explosive activity.

More specifically, piles of lava flows at the Kaukab locality are about 10 m thick at the centre, diminishing to 3 m in thickness at the edge of the plateau. The thickness of other piles of lava flows ranges from 7 m to 10 m at the localities of Feidat El-Meiza and Ein Abou Jema, to almost 20 m at Himmat El-Jazira. Based on their position on top of Pleistocene (Lower Quaternary) terraces, Ponikarov (1967) suggested that these lava flows are Upper Quaternary in age. More recent volcanic activity is indicated by the superposition of lava and scoria cones on these flows.

## 3. Methods of analysis

Whole rock major- and trace-element analyses were conducted at the Activation Laboratories (ACTLABS) in Ancaster, Ontario, Canada. The samples were run for major oxides on a combination of simultaneous and sequential Thermo Jarrell-Ash Enviro II ICP. Calibration was achieved using a combination of CANMET and USGS reference materials. Loss on ignition (LOI) was determined by heating powdered samples for 50 minutes.

For trace and rare earth element (REE) analyses, solutions of the fused samples prepared as above are spiked with three internal standards to cover the entire mass range. These are further diluted and are introduced into a Perkin Elmer-SCIEX Elan 6000 ICP/MS using a proprietary sample introduction methodology. The fusion process ensures total metals (particularly for elements like REE in resistate phases; this may not be the case for acid digestions, particularly for heavy REE and other elements, contained in refractory minerals like zircon, sphene or monazite). The primitive mantle values used for normalization are those of Sun & McDonough (1989).

The Sr and Nd isotopic analyses were conducted at McMaster University, Ontario, Canada. Before commencing the chemical procedures, sample powders were leached in 6M HCl for several hours in order to remove any traces of secondary Sr. Sr and Nd were separated in cation exchange columns; the separation was followed by purification in a second separation column according to the method of Richard, Shimizu & Allègre (1976). The solution of Nd was mounted on double filaments and measured on a VG Isolab-54 mass spectrometer with multiple collectors in dynamic mode. During the course of the study, the La Jolla Nd-standard gave $^{143}Nd/^{144}Nd = 0.51185$. The average precision of repetitions was $\pm 0.000015$ ($2\sigma$). The solution of Sr was mounted on a single filament and measured by a VG Isomass–354 with multiple collectors. The Sr isotopes were normalized for fractionation to $^{86}Sr/^{88}Sr = 0.1194$, related to a value of 0.710241 for the NBS-987 standard. The average precision of repetitions was $\pm 0.00002$ ($2\sigma$).

## 4. Petrography

Rocks of the Euphrates volcanic field are predominantly phyric, with olivine, clinopyroxene and/or plagioclase phenocrysts embedded in a microcrystalline to cryptocrystalline groundmass. The groundmass consists primarily of plagioclase laths, small grains of clinopyroxene, olivine and opaque phases, in addition to minor amounts of alteration products (mainly iddingsite). These mafic volcanic rocks exhibit a variety of textures, including intersertal, porphyritic, glomeroporphyritic, ophitic, sub-ophitic, pilotaxitic, vesicular and rarely aphyric.

Plagioclase makes up about 45 to 55 vol. % of the whole rock. It forms crystals that range in size from tiny microlites to large prisms, occurring mostly as groundmass material (0.05 to 0.5 mm long microlaths), and rarely as microphenocrysts or phenocrysts (0.6 to 1.2 mm long) which may contain micro-inclusions of apatite needles. Clinopyroxene forms anhedral to subhedral crystals, which often show sector zoning. It varies in colour from pale beige to lilac, forming about 30–35 vol. % of the whole rock. Clinopyroxene is also abundant both as a phenocryst and as a groundmass phase. The proportions of clinopyroxene existing as phenocryst versus groundmass phases are highly variable. Clinopyroxene is rarely twinned, and occasionally contains inclusions of plagioclase microlaths and opaque phases. Olivine crystals occur as subhedral to euhedral, large, equant and occasionally skeletal phenocrysts, and in the form of minute anhedral groundmass grains; olivine forms 15–20 vol. % of the whole rock. Corroded and embayed olivine phenocrysts are observed in several samples. The olivine phenocrysts are largely fresh, but in some rocks the olivine is partially altered to iddingsite. Olivine crystals generally contain inclusions of opaque phases. The latter also occur as small cubes or acicular needles within the groundmass.

## 5. Geochemistry

### 5.a. Major, trace and rare-earth element geochemistry

Major and trace element data for 17 representative samples of the Euphrates volcanic field of northeastern Syria are presented in Table 1. Rocks of this volcanic field are largely ultrabasic, as they have very low silica values (38.2 to 45.5 wt % $SiO_2$). They exhibit narrow

https://doi.org/10.1017/S0016756808004901 Published online by Cambridge University Press

Table 1. Major and trace element composition (in wt %, and ppm, respectively) of representative samples of the Euphrates volcanic field, northeastern Syria

| Sample | HJ-117 | HJ-127 | HJ-147 | HJ-77 | HJ-87 | FM-77 | FM-87 | FM-97 | EJ-17 | EJ-27 | KB-27 | KB-47 | KB-57 | KB-67 | KB-77 | KB-87 | KB-97 | Ave. |
|---|---|---|---|---|---|---|---|---|---|---|---|---|---|---|---|---|---|---|
| $SiO_2$ | 42.42 | 43.52 | 40.63 | 42.37 | 42.45 | 44.49 | 44.44 | 45.05 | 43.96 | 43.38 | 38.56 | 42.97 | 38.23 | 44.55 | 45.49 | 45.36 | 45.2 | 43.12 |
| $TiO_2$ | 3.34 | 3.1 | 3.2 | 3.19 | 3.21 | 2.89 | 2.45 | 2.63 | 2.68 | 2.65 | 3.49 | 2.8 | 3.35 | 2.51 | 2.53 | 2.62 | 2.63 | 2.90 |
| $Al_2O_3$ | 12.06 | 12.23 | 11.7 | 11.68 | 11.85 | 12.85 | 12.37 | 12.75 | 11.82 | 11.65 | 10.17 | 11.1 | 9.53 | 11.96 | 12.03 | 12.18 | 12.12 | 11.77 |
| $Fe_2O_3$* | 14.65 | 14.51 | 14.2 | 14.97 | 15.49 | 13.04 | 13.35 | 13.44 | 13.71 | 13.64 | 15.49 | 14.07 | 14.88 | 13.56 | 13.57 | 13.97 | 13.85 | 14.14 |
| MgO | 10.75 | 10.13 | 10.23 | 9.6 | 9.62 | 8.69 | 10.87 | 10.3 | 10.82 | 10.83 | 11.82 | 11.5 | 13.03 | 10.78 | 10.99 | 10.71 | 10.79 | 10.67 |
| MnO | 0.18 | 0.17 | 0.17 | 0.18 | 0.18 | 0.17 | 0.17 | 0.17 | 0.17 | 0.17 | 0.19 | 0.17 | 0.19 | 0.17 | 0.17 | 0.17 | 0.17 | 0.17 |
| CaO | 10.57 | 10.1 | 11.69 | 10.46 | 10.02 | 11.24 | 10.64 | 10.5 | 10.73 | 10.69 | 10.22 | 10.55 | 11.4 | 11.19 | 9.71 | 9.51 | 9.77 | 10.53 |
| $Na_2O$ | 2.49 | 3.03 | 2.49 | 2.4 | 2.67 | 2.31 | 2.91 | 2.69 | 3.7 | 3.41 | 5.23 | 3.66 | 4.14 | 2.87 | 3.21 | 3.3 | 3.33 | 3.17 |
| $K_2O$ | 1.29 | 1.15 | 1.13 | 1.1 | 1.27 | 1.18 | 0.95 | 1.02 | 1.14 | 1.28 | 1.87 | 1.14 | 1.29 | 0.92 | 1.09 | 1.15 | 1.16 | 1.18 |
| $P_2O_5$ | 0.57 | 0.52 | 0.56 | 0.72 | 0.74 | 0.49 | 0.38 | 0.43 | 0.72 | 0.64 | 1.4 | 0.73 | 1.07 | 0.56 | 0.6 | 0.57 | 0.6 | 0.66 |
| LOI | 1.21 | 0.46 | 3 | 2.83 | 1.87 | 2.54 | 0.91 | 1.15 | −0.38 | 0.77 | 0.49 | 0.41 | 1.68 | 0.6 | −0.61 | −0.62 | −0.36 | 0.94 |
| Total | 99.55 | 98.92 | 98.99 | 99.48 | 99.38 | 99.88 | 99.44 | 100.14 | 99.07 | 99.1 | 98.93 | 99.1 | 98.79 | 98.66 | 98.77 | 98.92 | 99.25 | 99.20 |
| Sc | 22 | 23 | 22 | 21 | 21 | 22 | 21 | 23 | 23 | 24 | 18 | 21 | 17 | 21 | 22 | 21 | 21 | 21 |
| V | 285 | 281 | 289 | 256 | 239 | 244 | 223 | 255 | 244 | 240 | 203 | 208 | 213 | 210 | 219 | 215 | 214 | 238 |
| Cr | 342 | 360 | 352 | 293 | 276 | 362 | 356 | 312 | 384 | 337 | 270 | 337 | 392 | 310 | 330 | 321 | 322 | 333 |
| Ni | 257 | 266 | 264 | 249 | 241 | 291 | 290 | 213 | 317 | 266 | 293 | 312 | 370 | 305 | 313 | 283 | 283 | 283 |
| Rb | 13 | 13 | 13 | 14 | 13 | 13 | 15 | 15 | 12 | 12 | 19 | 10 | 8 | 9 | 11 | 12 | 12 | 13 |
| Sr | 1141 | 885 | 817 | 1057 | 1106 | 888 | 754 | 779 | 655 | 614 | 1129 | 821 | 1032 | 720 | 696 | 696 | 709 | 853 |
| Ba | 195 | 201 | 278 | 218 | 205 | 243 | 228 | 248 | 235 | 234 | 246 | 189 | 181 | 179 | 175 | 189 | 186 | 214 |
| Zr | 186 | 173 | 185 | 228 | 224 | 201 | 195 | 160 | 133 | 144 | 276 | 225 | 268 | 179 | 180 | 194 | 197 | 197 |
| Nb | 41 | 38 | 41 | 47 | 46 | 47 | 45 | 33 | 25 | 28 | 67 | 45 | 71 | 38 | 37 | 39 | 40 | 43 |
| Y | 19 | 19 | 19 | 22 | 22 | 23 | 23 | 19 | 17 | 18 | 27 | 24 | 28 | 23 | 22 | 22 | 22 | 22 |
| Ga | 23 | 23 | 22 | 23 | 22 | 22 | 22 | 21 | 20 | 20 | 27 | 22 | 24 | 21 | 22 | 23 | 22 | 22 |
| Th | 2.99 | 2.88 | 2.9 | 3.74 | 3.74 | 3.95 | 3.89 | 3.1 | 2.26 | 2.52 | 5.58 | 3.73 | 5.82 | 3.2 | 3.04 | 3.27 | 3.17 | 3.52 |
| U | 0.63 | 0.77 | 0.89 | 0.99 | 1 | 1.03 | 1.06 | 0.62 | 0.45 | 0.47 | 1.61 | 1.27 | 1.27 | 0.93 | 0.88 | 0.87 | 0.92 | 0.92 |
| Hf | 4.7 | 4.2 | 4.4 | 5.5 | 5.1 | 4.7 | 4.5 | 3.9 | 3.4 | 3.7 | 5.5 | 5.5 | 5.5 | 4.3 | 4.2 | 5 | 4.7 | 4.6 |
| Ta | 2.49 | 2.6 | 2.38 | 2.88 | 2.79 | 2.74 | 2.57 | 2.07 | 1.47 | 1.69 | 4.17 | 2.73 | 4.37 | 2.26 | 2.17 | 2.41 | 2.35 | 2.60 |
| Mg no. | 0.65 | 0.63 | 0.64 | 0.61 | 0.61 | 0.62 | 0.67 | 0.65 | 0.66 | 0.66 | 0.65 | 0.67 | 0.68 | 0.66 | 0.67 | 0.65 | 0.66 | 0.65 |

$Fe_2O_3$* is total iron presented as $Fe_2O_3$, and Mg no. = (molar Mg/(Mg+$Fe^{2+}$)) assuming $Fe^{3+}/Fe^{2+} = 0.20$.

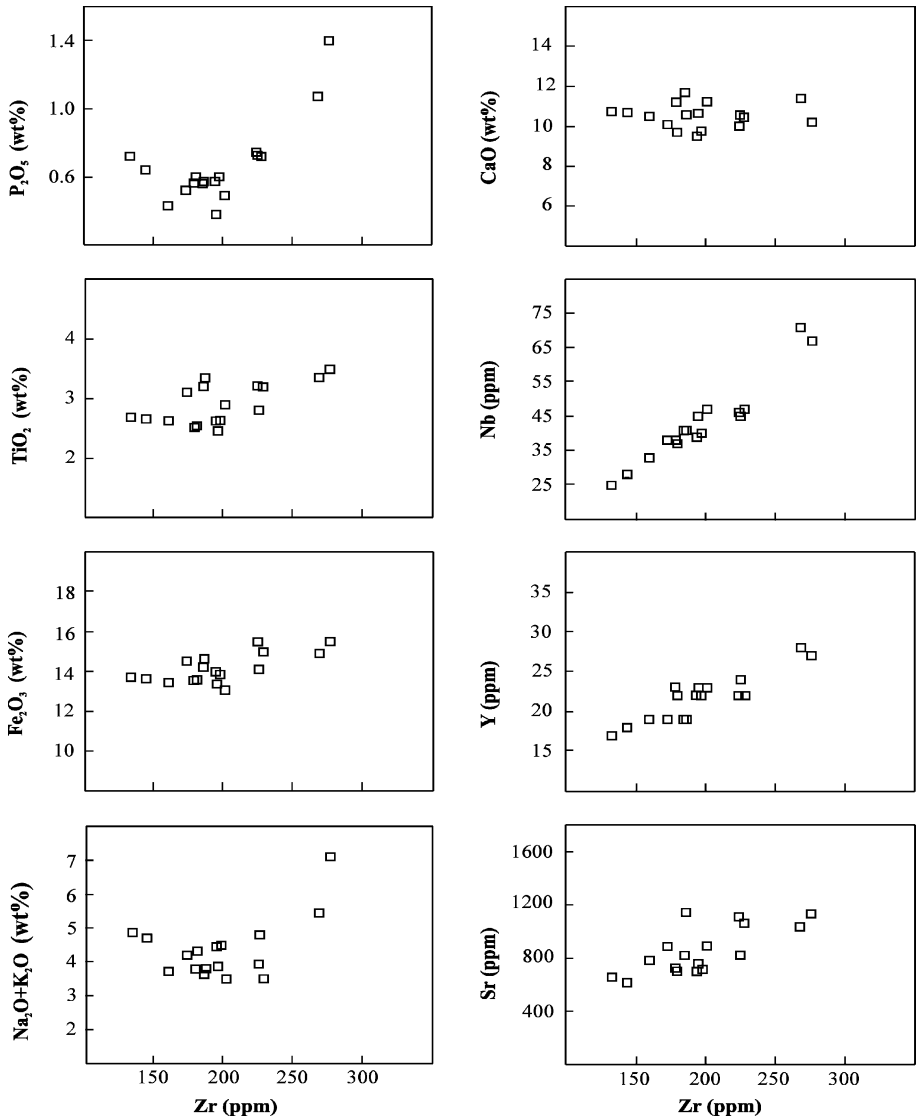


Figure 3. Variations of selected major and trace elements v. Zr within the Euphrates volcanic field of northeastern Syria.

major element compositional ranges: 9.5–12.9 wt % $Al_2O_3$, 8.7–13.0 wt % MgO, 13.0–15.5 wt % $Fe_2O_3$ (as total iron), 9.5–11.7 wt % CaO and 2.5–3.5 wt % $TiO_2$ (Table 1). Based on the total alkali versus silica diagram of Le Bas & Streckeisen (1991; not shown), the lavas are represented largely by nephelinites, basanites and alkali basalts. The Mg numbers (= molar $Mg/(Mg+Fe^{2+})$, assuming a $Fe^{3+}/Fe^{2+}$ ratio of 0.2) range from 0.61 to 0.68 (with an average of 0.65). These values indicate that the magma may have experienced some degree of olivine and clinopyroxene fractionation.

The Euphrates volcanic rocks also exhibit a relatively narrow trace element compositional range: Cr = 270–392 ppm, V = 203–289 ppm, Sr = 614–1140 ppm, Ba = 175–278 ppm, and Rb = 8–19 ppm, and are generally enriched in the high field strength elements (HFS) such as Zr (133–276 ppm), Y (17–28 ppm) and Nb (25–71 ppm; Table 1). Rocks of the investigated volcanic field exhibit elemental ratios, such as La/Nb (0.77), Zr/Nb (4.6), and Rb/Nb (0.30), similar to the average of some OIB lavas (La/Nb = 0.72, Zr/Nb = 4.1, and Rb/Nb = 0.37; Weaver, 1991).

Variation diagrams of major elements versus Zr (Fig. 3) indicate that $P_2O_5$, $TiO_2$, total iron (as $Fe_2O_3$) and alkalis increase with increasing Zr, whereas CaO remains somewhat constant. Trace elements exhibit well-defined correlations with Zr; Nb, Y and Sr show a gradual increase with increasing Zr (Fig. 3). Since Zr and Y are incompatible in the main fractionating phases of basaltic magmas (olivine, pyroxene and plagioclase), the Zr/Y ratio is not normally affected by moderate amounts of fractional crystallization. However, as Zr is more incompatible in mantle phases than Y, the Zr/Y ratio tends to be higher when the degree of melting is small; variation of Zr/Y with Zr can thus be used to illustrate petrogenetic processes such as partial melting. The positive correlation of Zr/Y with Zr obtained for the Euphrates lavas (not shown) suggests that partial melting processes have played a significant role in producing the range of magma compositions observed (see Section 6). These

https://doi.org/10.1017/S0016756808004901 Published online by Cambridge University Press

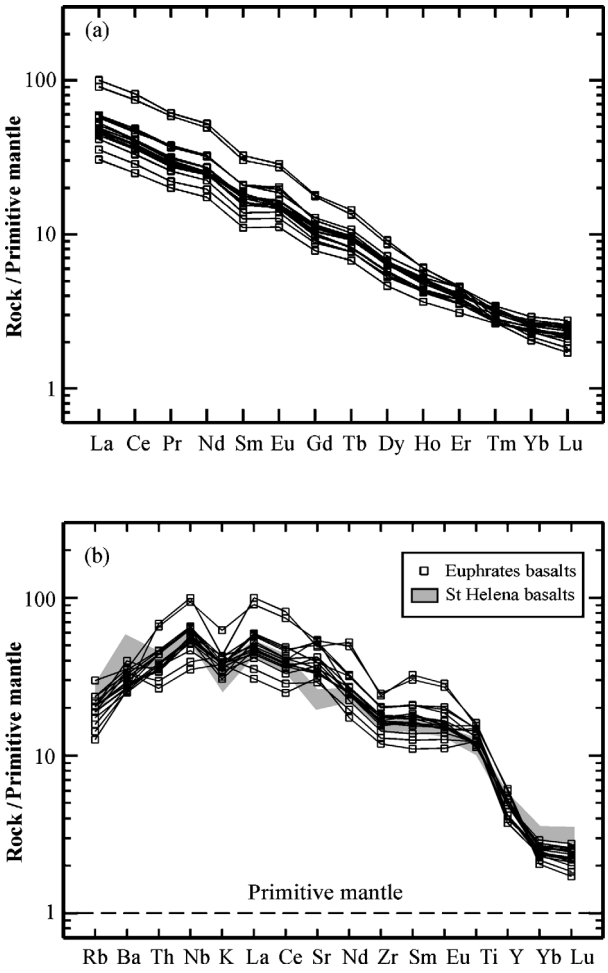


Figure 4. (a) Primitive mantle-normalized rare-earth-element (REE) patterns of the Euphrates volcanic field. (b) Primitive mantle-normalized incompatible element patterns for the Euphrates lavas, superimposed on an envelope representing the St Helena alkali basalts, which are plotted for comparison. Normalization values used are from Sun & McDonough (1989). Data on the St Helena alkali basalts are taken from Chaffey, Cliff & Wilson (1989). Note the similarity of the patterns between the two suites.

trace elements, combined with the geological setting, confirm the within-plate character of the investigated Euphrates lavas.

The rare earth element compositions of seventeen samples from the Euphrates volcanic field are given in Table 2. The rocks are generally enriched in REE relative to primitive mantle, with the sum of REE ranging from 113 to 344 ppm. Primitive mantle-normalized REE patterns are illustrated in Figure 4a. Overall, the REE patterns are parallel to subparallel and strongly fractionated ($(La/Yb)_N = 19.6$). The two nephelinite samples that possess the lowest $SiO_2$ contents (38.2 and 38.6 wt % $SiO_2$) have significantly higher LREE concentrations than the other samples. This is, most likely, the result of differences in the degrees of partial melting of the mantle source rock (see Section 6).

The primitive mantle-normalized incompatible element patterns of the Euphrates volcanic field (Fig. 4b)

Table 2. Rare earth element (REE) composition (in ppm) of the Euphrates volcanic field, northeastern Syria

| Sample | HJ-117 | HJ-127 | HJ-147 | HJ-77 | HJ-87 | EJ-17 | EJ-27 | FM-77 | FM-87 | FM-97 | KB-27 | KB-47 | KB-57 | KB-67 | KB-77 | KB-87 | KB-97 | Ave. |
|---|---|---|---|---|---|---|---|---|---|---|---|---|---|---|---|---|---|---|
| La | 33.6 | 30.1 | 33 | 40 | 39.2 | 35.2 | 36.3 | 28.5 | 21 | 24.3 | 62.2 | 40.8 | 68.8 | 32 | 31 | 32.7 | 31.6 | 33.0 |
| Ce | 71.2 | 63.3 | 66.9 | 83.7 | 81.4 | 72.8 | 73.3 | 58.6 | 44.2 | 50.7 | 132 | 86.1 | 145 | 67 | 64.9 | 68.4 | 67.6 | 68.4 |
| Pr | 8.34 | 7.54 | 7.68 | 10.08 | 10.42 | 8.73 | 8.56 | 7.09 | 5.51 | 6.09 | 16.11 | 10.34 | 16.89 | 8.01 | 7.8 | 8.12 | 8.06 | 8.22 |
| Nd | 34.5 | 32.8 | 33.1 | 43.3 | 44.1 | 36.9 | 36.4 | 30.3 | 23.5 | 26.5 | 66.7 | 43.1 | 70.7 | 33.3 | 33.6 | 34.5 | 33.8 | 35.0 |
| Sm | 7.96 | 7.21 | 7.13 | 9.24 | 9.19 | 7.8 | 7.54 | 6.11 | 4.9 | 5.59 | 13.4 | 9.29 | 14.4 | 6.85 | 7.05 | 8.17 | 7.62 | 7.45 |
| Eu | 2.585 | 2.474 | 2.455 | 3.398 | 3.283 | 2.786 | 2.755 | 2.335 | 1.867 | 2.128 | 4.565 | 3.121 | 4.797 | 2.529 | 2.599 | 2.613 | 2.548 | 2.660 |
| Gd | 6 | 5.97 | 5.82 | 7.35 | 7.34 | 6.87 | 6.7 | 5.42 | 4.66 | 5.23 | 10.5 | 7.62 | 10.7 | 6.19 | 6.53 | 6.75 | 6.27 | 6.24 |
| Tb | 0.89 | 0.88 | 0.89 | 1.1 | 1.1 | 1.05 | 1.01 | 0.83 | 0.73 | 0.83 | 1.45 | 1.16 | 1.55 | 0.99 | 1 | 1.03 | 0.99 | 0.94 |
| Dy | 4.27 | 4.19 | 4.2 | 4.91 | 4.96 | 4.88 | 4.89 | 3.9 | 3.42 | 4.01 | 6.36 | 5.33 | 6.73 | 4.64 | 4.72 | 4.91 | 4.81 | 4.40 |
| Ho | 0.72 | 0.69 | 0.69 | 0.79 | 0.82 | 0.85 | 0.83 | 0.7 | 0.6 | 0.71 | 1 | 0.92 | 0.99 | 0.82 | 0.78 | 0.86 | 0.78 | 0.74 |
| Er | 1.82 | 1.82 | 1.7 | 1.85 | 1.86 | 1.96 | 1.91 | 1.71 | 1.49 | 1.72 | 2.16 | 2.15 | 2.21 | 1.92 | 1.92 | 2.17 | 2.02 | 1.79 |
| Tm | 0.202 | 0.197 | 0.199 | 0.201 | 0.21 | 0.232 | 0.237 | 0.205 | 0.196 | 0.226 | 0.198 | 0.238 | 0.214 | 0.247 | 0.242 | 0.254 | 0.23 | 0.21 |
| Yb | 1.13 | 1.19 | 1.15 | 1.18 | 1.23 | 1.31 | 1.27 | 1.25 | 1.16 | 1.26 | 1.01 | 1.3 | 1.07 | 1.29 | 1.32 | 1.44 | 1.37 | 1.21 |
| Lu | 0.156 | 0.167 | 0.148 | 0.164 | 0.156 | 0.183 | 0.188 | 0.175 | 0.162 | 0.187 | 0.127 | 0.18 | 0.136 | 0.181 | 0.192 | 0.204 | 0.192 | 0.167 |
| ∑REE | 173.4 | 158.5 | 165.1 | 207.3 | 205.3 | 181.6 | 181.9 | 147.1 | 113.4 | 129.5 | 317.8 | 211.6 | 344.2 | 166.0 | 163.7 | 172.1 | 167.9 | 170.4 |

https://doi.org/10.1017/S0016756808004901 Published online by Cambridge University Press

Table 3. Sr and Nd isotopic composition of representative samples from the Euphrates volcanic field, northeastern Syria

| Sample | $^{87}Sr/^{86}Sr$ | $^{143}Nd/^{144}Nd$ | $\varepsilon_{Nd}$ |
|---|---|---|---|
| HJ-127 | 0.703330 | 0.512888 | 4.88 |
| FM-87 | 0.703520 | 0.512868 | 4.49 |
| EJ-17 | 0.703520 | 0.512929 | 5.68 |
| KB-47 | 0.703090 | 0.512940 | 5.89 |
| KB-87 | 0.703130 | 0.512908 | 5.27 |

indicate that the rocks are enriched in the large ion lithophile (LIL) elements (K, Rb, Ba, Th and the LREE) and the incompatible HFS elements Nb, Zr and Ti relative to primitive mantle normalizing abundances. A comparison with trace element profiles of the St Helena alkali basalts (which are typical of HIMU-OIB: Chaffey, Cliff & Wilson, 1989) show that the Euphrates lavas are similar in trace-element composition (Fig. 4b). Thus, the overall chemical traits of the investigated lavas reflect strong affinities to OIB. According to Pearce *et al.* (1990), melting of 'plume' asthenosphere, or lithosphere enriched by small volume melts from the asthenosphere produces 'humped' patterns with Ba, Th and Nb the most enriched elements and the degree of enrichment directly relating to the degree of incompatibility. The marked depletion of Y and the heavy REE in the Euphrates lavas may indicate that garnet was a residual phase during the partial melting event. Thus, the Euphrates lavas can be interpreted in terms of a garnet-bearing mantle source (see Section 6).

### 5.b. Nd and Sr isotopes

The $^{143}Nd/^{144}Nd$ ratios of representative samples from the Euphrates volcanic field range from $0.512868 \pm 1$ to $0.512940 \pm 1$ ($\varepsilon_{Nd} = 4.5$ to 5.9), whereas the $^{87}Sr/^{86}Sr$ ratios range from $0.703090 \pm 2$ to $0.703520 \pm 2$ (Table 3). The isotopic compositions are plotted in Figure 5, along with data from other alkali basaltic suites. Also plotted in this diagram (Fig. 5) are the compositions of various mantle reservoirs (EMI, EMII, HIMU and N-MORB), taken from Hart (1988); EMI ('enriched mantle 1') and EMII ('enriched mantle 2') types of OIB may represent the addition of small amounts of subducted sediments; pelagic in the case of EMI and terrigenous in the case of EMII (Weaver, 1991; Hofmann, 1997). HIMU ('high $\mu$') refers to a high $^{238}U/^{204}Pb$ ($\mu$) mantle end-member, and has the lowest $^{87}Sr/^{86}Sr$ of any OIB (Hofmann, 1997), which is thought to be derived from subducted basaltic oceanic crust. Examples of HIMU-OIB are St Helena, Bouvet, Ascension, Austral Islands, Balleny Islands and the Azores; typical EMI-OIB are Tristan da Cunha, Gough, Kerguelen and Pitcairn; EMII-OIB: Society Islands, Samoa, Tutuila and Upolu (Weaver, 1991; Hofmann, 1997).

Rocks of the Euphrates volcanic field are, as shown in Figure 5, isotopically similar to some Golan–Galilee alkali basalts (Weinstein *et al.* 2006), Jordanian alkali basalts (Shaw *et al.* 2003), Lebanese Cenozoic alkali basalts (Abdel-Rahman & Nassar, 2004), and to the Mesozoic alkali basalts of the Middle East (Laws & Wilson, 1997; Abdel-Rahman, 2002). The investigated lavas also exhibit isotopic compositions similar to the St Helena alkali basalts (Staudigel *et al.* 1984; Hofmann, 1997) as they exhibit relatively high initial $^{143}Nd/^{144}Nd$ and low initial $^{87}Sr/^{86}Sr$ isotopic ratios, and are thus distinct from EMI-OIB and EMII-OIB (e.g. Weaver, 1991; Wilson, 1993). It should be noted that the St Helena alkali basalts and the Lebanese lavas were interpreted to represent small-degree partial melts of upper mantle material (Weaver, 1991; Abdel-Rahman & Nassar, 2004).

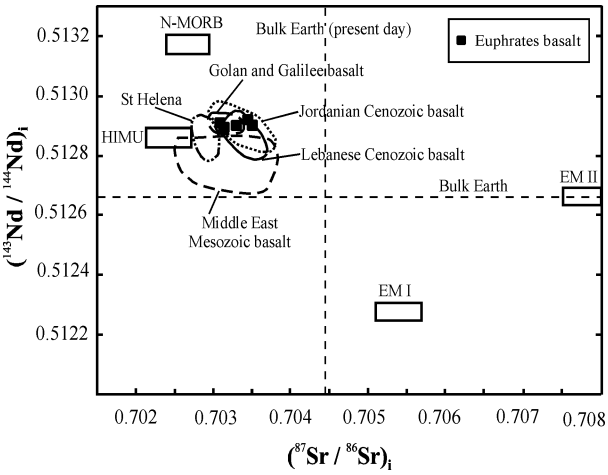


Figure 5. $(^{87}Sr/^{86}Sr)_i$ v. $(^{143}Nd/^{144}Nd)_i$ ratios for the Euphrates volcanic field of northeastern Syria (closed squares). Compositions of EMI, EMII, HIMU and N-MORB are from Hart (1988). Fields for the St Helena basalts from Staudigel *et al.* (1984), Golan–Galilee alkali basalts from Weinstein *et al.* (2006), Jordanian alkali basalts from Shaw *et al.* (2003), Lebanese Cenozoic alkali basalts from Abdel-Rahman & Nassar (2004), and the Middle East Mesozoic basalts from Laws & Wilson (1997) and Abdel-Rahman (2002).

## 6. Discussion

### 6.a. Role of crustal contamination

On the variation diagram of Ta/Yb versus Th/Yb (after Pearce, 1983), the Euphrates volcanic rocks plot along the diagonal trend of mantle spectrum, and away from the trend of crustal contamination (Fig. 6). This diagram shows also that the examined rocks overlap with some Golan–Galilee alkali basalts (taken from Weinstein *et al.* 2006), but the Lebanese Cenozoic alkali basalts (Abdel-Rahman & Nassar, 2004) plot slightly off this trend. The degree of contamination that silicate melts may have experienced can be assessed via the use of certain chemical parameters. For example, basaltic lavas affected by crustal contamination exhibit K/P ratios > 7, La/Ta > 22, and La/Nb > 1.5 (e.g. Hart *et al.* 1989). The low values of such elemental ratios in rocks of the Euphrates volcanic field (K/P 3.4, La/Ta 13, La/Nb 0.77, on average), along with their Sr–Nd isotopic composition, and their low silica

https://doi.org/10.1017/S0016756808004901 Published online by Cambridge University Press

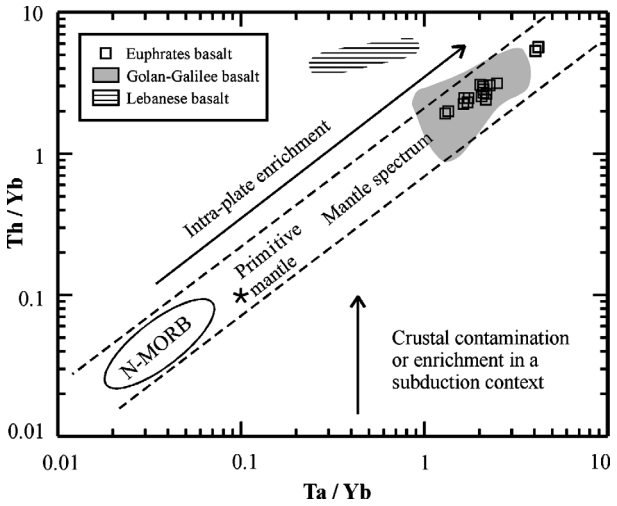


Figure 6. Ta/Yb v. Th/Yb diagram (after Pearce, 1983) showing that the Euphrates lavas plot along the diagonal trend of the mantle spectrum, being distinct from the crustal contamination trend (see text for details). Fields representing Golan–Galilee and Lebanese Cenozoic alkali basalts are from Weinstein *et al.* (2006) and Abdel-Rahman & Nassar (2004), respectively.

values (43.1 wt % $SiO_2$, on average), all suggest that the magma was subjected to minimal crustal contamination. Magma ascent may have been rapid enough from the site of partial melting to the surface to escape contamination. As pointed out by Smith *et al.* (1999), the Nd content of most lower crustal xenoliths is too low (usually < 10 ppm) to significantly change Nd-isotopic values without adding 70 % to 85 % lower crustal material. Such a large amount of contamination by crustal material is thermodynamically difficult because a considerable amount of heat is required to assimilate crustal rocks, and the magma would then cool quickly and perhaps 'freeze' in place. Moreover, this would have resulted in the presence of some lower crustal xenoliths within the lava flows, but the Euphrates lava flows contain no such crustal xenoliths.

Based on geological and geophysical data, Sawaf *et al.* (1993) showed that a slight crustal thinning is present, going from 37 km south and north of the Euphrates graben to 35 km beneath it. The occurrence of the Euphrates volcanic field within such a tensional stress field is consistent with a lack of significant crustal contamination in these lavas; the lower $^{87}Sr/^{86}Sr$ ratios (0.70309 to 0.70352) of the Euphrates lavas could represent mantle source values. Thus, the geochemical and field characteristics, along with the nature of tectonism (extensional), suggest that the role of crustal contamination during magma evolution has been minimal.

### 6.b. Source characteristics and possible depth of melting

In terms of their Zr, Nb and Y compositions (Fig. 7a), the Euphrates lavas plot just above the plume-related mid-ocean ridge basalt (P-MORB), as they exhibit relatively higher concentrations of Zr, but lower concentrations of Y than transitional-, or normal-

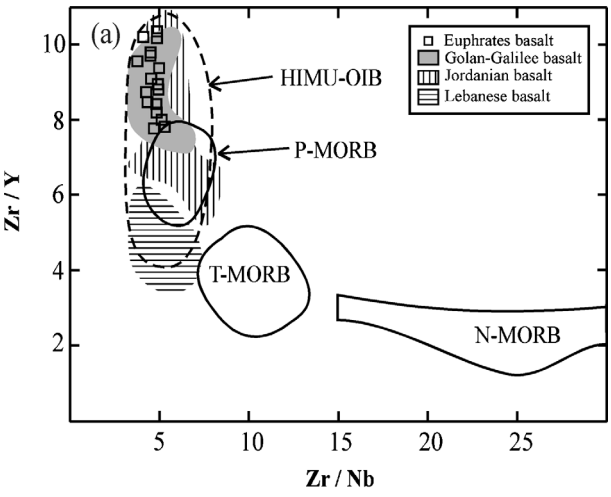


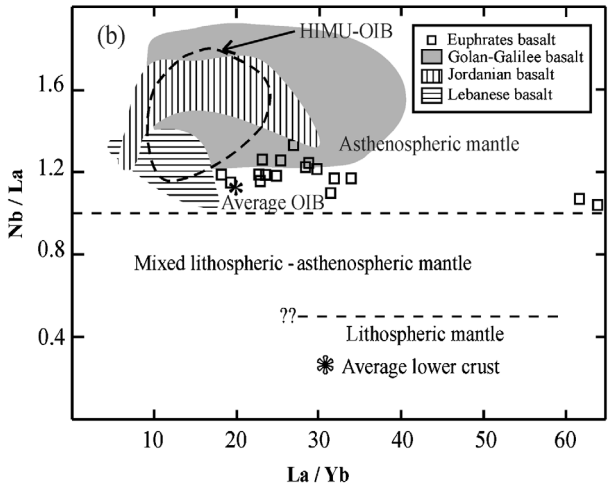


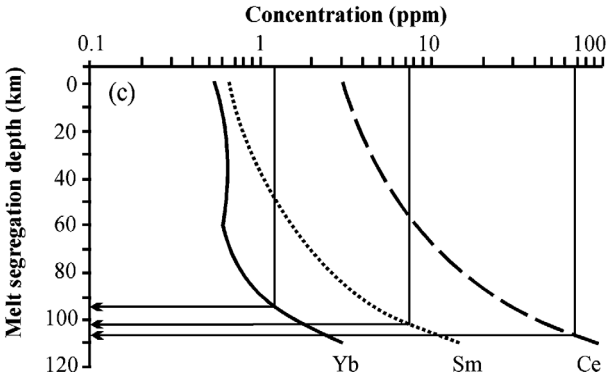


Figure 7. (a) Zr/Y v. Zr/Nb diagram showing that the Euphrates volcanic field of northeastern Syria plots just above the field of fertile, plume-related MORB (P-MORB). The other fields are transitional MORB (T-MORB) and normal MORB (N-MORB) and are taken from Menzies & Kyle (1990). The field delineating HIMU-OIB is taken from Abdel-Rahman (2002). Data representing Golan–Galilee, Jordanian and Lebanese Cenozoic alkali basalts are from Weinstein *et al.* (2006), Shaw *et al.* (2003) and Abdel-Rahman & Nassar (2004), respectively. (b) Nb/La v. La/Yb variation diagram. The composition of the Euphrates lavas (relatively low La/Yb and high Nb/La) suggests an OIB-like asthenospheric mantle source. Average OIB is after Fitton, James & Leeman (1991), and average lower crust (representing average of six lower crustal granulite xenoliths) is after Chen & Arculus (1995). The source of the other data fields shown is given in Figure 7a above. The field of HIMU-OIB, and

https://doi.org/10.1017/S0016756808004901 Published online by Cambridge University Press

MORB (T-MORB or N-MORB: Menzies & Kyle, 1990; Melluso *et al.* 1995). The examined rocks overlap with those representing the Golan–Galilee and Jordanian alkali basalts of Weinstein *et al.* (2006) and Shaw *et al.* (2003), respectively, but exhibit higher Zr/Y ratios than the Lebanese Cenozoic alkali basalts of Abdel-Rahman & Nassar (2004).

The Euphrates lavas also exhibit elemental ratios ((Zr/Nb) = 4.6, (La/Nb) = 0.77, (Ba/Th) = 61, and (Rb/Nb) = 0.30, on average), similar to those characteristic of OIB (Weaver, 1991). Niobium, along with some other HFS elements, is found to be highly variable in lithospheric mantle melts. Thus, variations in the La/Nb ratios have been interpreted by some authors to reflect the style of metasomatic enrichment (small fraction convection mantle melt, or subduction-related metasomatism: Gibson *et al.* 1995). Considering the within-plate character of the Euphrates volcanic field, subduction-related metasomatism was an unlikely process in the region during Cenozoic times. Bradshaw & Smith (1994) and Smith *et al.* (1999) have suggested that, since HFS elements (such as Nb) are depleted in the lithospheric mantle relative to the light REE (e.g. La), high Nb/La ratios (approximately > 1) indicate an OIB-like asthenospheric mantle source for basaltic magmas, and lower ratios (approximately < 0.5) indicate a lithospheric mantle source. The Nb/La and La/Yb ratios (averages of 1.3 and 27, respectively) are consistent with an asthenospheric mantle (OIB-like) source (Fig. 7b): the Euphrates lavas plot in the field of asthenospheric mantle and near average OIB. Similarly, the Golan–Galilee, the Jordanian and the Lebanese Cenozoic alkali basalts (Weinstein *et al.* 2006; Shaw *et al.* 2003; Abdel-Rahman & Nassar, 2004, respectively), plot in the field of asthenospheric mantle. Thus, trace element and isotopic data suggest that the investigated lavas have chemical characteristics similar to OIB (Fig. 7a), and were possibly derived from an asthenospheric mantle source. The relatively uniform $^{143}Nd/^{144}Nd$ ratios ($\varepsilon_{Nd} = 4.5$ to 5.9) for the Euphrates volcanic field suggest that its magma was developed by partial melting of an isotopically uniform mantle source.

The presence of garnet as a residual phase in the source region of the lavas can be inferred from: (1) fractionation of the heavy rare-earth elements (HREE; McKenzie & O'Nions, 1991; cf. Fig. 4a), and (2) the greater than chondritic Dy/Yb ratio (1.57); the Euphrates lavas have an average Dy/Yb ratio of 3.64. These rocks also have an average $(Tb/Yb)_N$ ratio of 3.5, which is slightly higher than that of the alkali basalts of Hawaii ($(Tb/Yb)_N$ range from 1.9 to 2.5); the Hawaiian basalts are considered to have been derived from a garnet-bearing mantle source (McKenzie & O'Nions, 1991; Frey *et al.* 1991, 2000). Further south, the source of the alkali basalts and basanites of the Jordanian Miocene to Recent lavas were related to melts of deep garnet-bearing lithospheric mantle, mixed with asthenospheric mantle melts (Shaw *et al.* 2003). These basaltic melts were formed in response to a phase of lithospheric extension. It should be noted that Shaw *et al.* (2003) concluded that the Afar plume of Ethiopia has not been channelled northwestwards beneath the Arabian plate, and played no role in producing the Arabian or Jordanian volcanic fields.

Using the study of Ellam (1992) on the estimation of depths of melt segregation, curves corresponding to the Ce, Sm and Yb concentrations of the Euphrates lavas (Fig. 7c) indicate a melt segregation depth ranging from about 94 to 108 km (that is, within the garnet lherzolite zone), consistent with an asthenospheric mantle source as indicated in Figure 7b. It should be noted that the transition from garnet to spinel peridotite takes place between a depth of about 60 to 80 km for normal mantle and about 80 to 100 km within hot mantle plumes (McKenzie & O'Nions, 1991; Lassiter, DePaolo & Mahoney, 1995).

### 6.c. Petrogenesis of the Euphrates lavas

It is well established that the geochemical signatures of basaltic magmas rely on three principal factors: (1) the composition of the mantle source including the presence or absence of a volatile phase ($H_2O + CO_2$), (2) the percentage of fusion and (3) the pressure conditions (depth) of the system subject to fusion. Thus, the nature of the mantle source material, whether it is dominated by recycled oceanic or continental crust, or by recycled sedimentary components, and the processes associated with melting and melt migration determine the composition of lavas. A number of studies, including those of White (1985), Allègre *et al.* (1987), Hart (1988), Weaver (1991), Gibson *et al.* (1997), Abdel-Rahman & Kumarapeli (1999), Frey *et al.* (2000), Gibb & Henderson (2006), Furman *et al.* (2006) and Weinstein *et al.* (2006), reflect that mafic alkaline lavas are diverse geochemically and form by partial melting of a range of mantle sources. In order to assess the role of petrogenetic processes such as partial melting, modelling was performed (using the batch melting equations of Shaw, 1970 and Allègre & Minister, 1978), and the calculations were done using two model source compositions: (1) primitive mantle taken from Sun & McDonough (1989) and (2) a mixed (50 % primitive–50 % depleted) mantle source of McKenzie & O'Nions (1991). Spinel, garnet and clinopyroxene were assumed to decrease in abundance linearly with increasing degrees of partial melting, as they are typically consumed at less than 25 %

the dashed lines separating fields of the asthenospheric, lithospheric and mixed mantle are taken from Abdel-Rahman (2002). (c) Model Ce, Sm and Yb concentrations in melts generated by partial melting and ranges of final melt segregation depths (model curves are after Ellam, 1992). The compositions of the Euphrates lavas (marked by vertical lines) indicate final melt segregation at depths between 94 and 108 km.

https://doi.org/10.1017/S0016756808004901 Published online by Cambridge University Press

Table 4. Model parameters used for batch partial melting calculations

| | Starting mode | | | Melt mode | | |
|---|---|---|---|---|---|---|
| Phase | a | b | c | a | b | c |
| Olivine | 0.570 | 0.550 | 0.55 | 0.15 | 0.05 | 0.15 |
| Opx | 0.235 | 0.220 | 0.22 | 0.15 | 0.05 | 0.15 |
| Cpx | 0.160 | 0.160 | 0.16 | 0.35 | 0.30 | 0.35 |
| Garnet | 0.000 | 0.035 | 0.07 | 0.00 | 0.30 | 0.35 |
| Spinel | 0.035 | 0.035 | 0.00 | 0.35 | 0.30 | 0.00 |

See notes for Table 5.

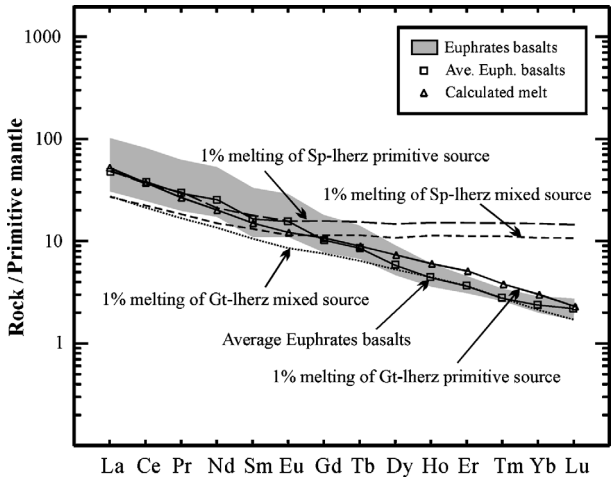


Figure 8. Calculated REE patterns for melts derived by batch partial melting of a primitive mantle composition with REE concentrations from Sun & McDonough (1989) and of a mixed source (50 % primitive/50 % depleted mantle) with REE concentrations from McKenzie & O'Nions (1991). The mantle mineral assemblages and melting proportions used are listed in Tables 4 and 5. The calculations were made using the Kds of McKenzie & O'Nions (1991), for degrees of partial melting (F) = 1 %, 2 % and 3 %. Normalization values used are taken from Sun & McDonough (1989). The calculated REE pattern produced by 1 % melting of a primitive garnet lherzolite source shows a reasonable fit with that of the average Euphrates lavas.

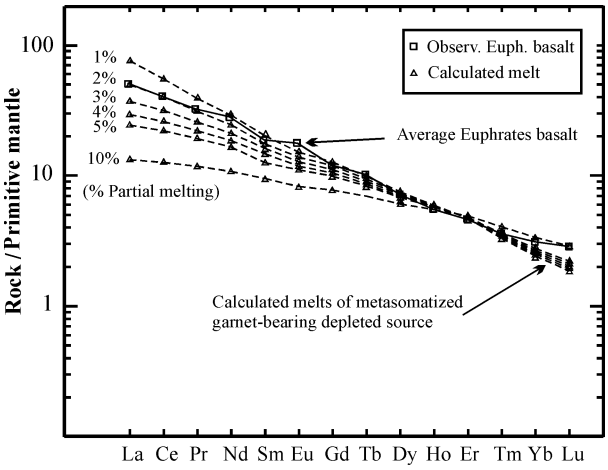


Figure 9. Calculated REE patterns for melts derived by batch partial melting of a garnet-bearing depleted source enriched with 5 % addition of metasomatizing fluids derived from a similar depleted source by 0.5 % melting. For the chemical compositions of mantle source materials used, and the partition coefficients of the various elements, we have used values of McKenzie & O'Nions (1991) for degrees of partial melting (F) = 1 % to 10 %. The mantle mineral assemblages and melting proportions used are listed in Table 6. Primitive mantle values used for normalization are taken from Sun & McDonough (1989). The calculated REE pattern produced by 2 % melting of the mantle source material given above shows a reasonable fit with that of the average Euphrates lavas.

partial melting (McKenzie & O'Nions, 1991; Lassiter, DePaolo & Mahoney, 1995).

Model and melting proportions are given in Tables 4 and 5 and are in line with those used in other partial melting calculations (e.g. Hanson, 1980; McKenzie & O'Nions, 1991; Witt-Eickschen & Kramm, 1997; Abdel-Rahman, 2002). Modelling was performed using three different mantle mineral assemblages: spinel lherzolite, garnet lherzolite and spinel–garnet lherzolite, for both a primitive and a mixed source composition. The partition coefficients used are from McKenzie & O'Nions (1991). Partial melting calculations were performed for 1 %, 2 % and 3 % partial melting. The results of the modelling (Tables 4, 5; Fig. 8) show that melting of a spinel-bearing source overestimates the HREE, and melting of a mixed source yields much lower LREE concentrations. Thus, neither depleted nor mixed primitive/depleted mantle material represents the mantle source for the Euphrates lavas and garnet is a required phase, but possibly with some minor spinel. The REE pattern of the calculated liquid produced by 1 % batch partial melting of garnet lherzolite (of a primitive mantle composition) produces a reasonable fit, as it closely matches that of the average Euphrates volcanic rocks (Fig. 8).

Another modelling scenario has also been considered. Similar to the model suggested by Pearce *et al.* (1990) for the Karacadağ volcanic plateau of southern Turkey, this modelling scenario is based on the assumption that the source is a mantle lithosphere, which was enriched in incompatible trace elements by metasomatism. The metasomatizing fluids could derive from either upwelling of a very deep primitive source such as garnet lherzolite, or by lateral migration from a MORB-like depleted source. The percolation of such fluids through the Euphrates lithospheric mantle source may have led to its enrichment in trace elements. With no geophysical or structural evidence of upwelling, the metasomatizing fluids may have been generated from a similarly depleted source by a very limited percentage of partial melting, which would be needed to reproduce the observed enrichment in incompatible elements. Thus, for this modelling attempt, the calculations were performed for 0.1 % to 10 % partial melting, using a variety of mantle source materials with variable mineralogies, and a number of different scenarios involving metasomatized sources. For the chemical compositions of mantle sources and the partition coefficients of the various elements, we have used values of McKenzie & O'Nions (1991). Model parameters, melting proportions and results are given in Table 6 and Figure 9. Within

https://doi.org/10.1017/S0016756808004901 Published online by Cambridge University Press

Table 5. Results of batch partial melting petrogenetic modeling using various mineralogical and chemical compositions of primitive and mixed mantle sources

| REE | 1 | 2 | 3 | 4 | 5 | 6 | 7 | 8 | 9 | 10 | 11 | 12 | 13 | 14 | 15 | 16 | 17 | 18 | 19 |
|---|---|---|---|---|---|---|---|---|---|---|---|---|---|---|---|---|---|---|---|
| La | 19.42 | 12.93 | 9.69 | 19.11 | 12.79 | 9.61 | 19.12 | 12.79 | 9.61 | 35.30 | 23.50 | 17.61 | 34.74 | 23.25 | 17.46 | 17.47 | 23.25 | 34.75 | 33.0 |
| Ce | 39.83 | 29.27 | 23.13 | 38.85 | 28.74 | 22.80 | 38.35 | 28.49 | 22.66 | 66.64 | 48.96 | 38.69 | 64.99 | 48.07 | 38.14 | 37.91 | 47.66 | 64.16 | 68.4 |
| Pr | 5.13 | 4.05 | 3.34 | 4.89 | 3.91 | 3.25 | 4.71 | 3.79 | 3.17 | 7.80 | 6.16 | 5.08 | 7.44 | 5.94 | 4.946 | 4.83 | 5.77 | 7.16 | 8.22 |
| Nd | 20.91 | 17.38 | 14.86 | 19.70 | 16.58 | 14.30 | 18.70 | 15.90 | 13.82 | 29.87 | 24.82 | 21.23 | 28.14 | 23.68 | 20.43 | 19.74 | 22.71 | 26.71 | 35.0 |
| Sm | 6.01 | 5.15 | 4.50 | 5.33 | 4.67 | 4.16 | 4.78 | 4.26 | 3.83 | 8.21 | 7.03 | 6.15 | 7.28 | 6.39 | 5.68 | 5.24 | 5.82 | 6.53 | 7.45 |
| Eu | 1.96 | 1.72 | 1.52 | 1.69 | 1.52 | 1.38 | 1.47 | 1.35 | 1.24 | 2.68 | 2.35 | 2.08 | 2.30 | 2.07 | 1.88 | 1.69 | 1.84 | 2.01 | 2.66 |
| Gd | 7.08 | 6.19 | 5.50 | 5.64 | 5.14 | 4.71 | 4.64 | 4.31 | 4.02 | 9.64 | 8.42 | 7.48 | 7.67 | 6.99 | 6.42 | 5.48 | 5.87 | 6.31 | 6.24 |
| Tb | 1.26 | 1.11 | 0.99 | 0.92 | 0.85 | 0.79 | 0.71 | 0.68 | 0.64 | 1.68 | 1.48 | 1.32 | 1.23 | 1.14 | 1.06 | 0.85 | 0.90 | 0.95 | 0.94 |
| Dy | 8.04 | 7.13 | 6.395 | 5.38 | 5.09 | 4.82 | 3.97 | 3.83 | 3.69 | 10.83 | 9.59 | 8.60 | 7.24 | 6.85 | 6.49 | 4.97 | 5.15 | 5.35 | 4.40 |
| Ho | 1.90 | 1.67 | 1.49 | 1.09 | 1.05 | 1.01 | 0.75 | 0.73 | 0.71 | 2.49 | 2.20 | 1.96 | 1.43 | 1.38 | 1.32 | 0.94 | 0.96 | 0.98 | 0.74 |
| Er | 5.52 | 4.86 | 4.33 | 2.79 | 2.73 | 2.66 | 1.82 | 1.80 | 1.78 | 7.37 | 6.49 | 5.79 | 3.73 | 3.64 | 3.55 | 2.38 | 2.41 | 2.43 | 1.79 |
| Tm | 0.85 | 0.75 | 0.66 | 0.35 | 0.35 | 0.34 | 0.21 | 0.21 | 0.21 | 1.12 | 0.99 | 0.88 | 0.46 | 0.46 | 0.45 | 0.28 | 0.28 | 0.28 | 0.21 |
| Yb | 5.42 | 4.78 | 4.27 | 1.85 | 1.88 | 1.90 | 1.08 | 1.10 | 1.11 | 7.42 | 6.54 | 5.85 | 2.53 | 2.57 | 2.61 | 1.52 | 1.50 | 1.48 | 1.21 |
| Lu | 0.81 | 0.72 | 0.64 | 0.23 | 0.24 | 0.24 | 0.13 | 0.13 | 0.13 | 1.07 | 0.95 | 0.85 | 0.30 | 0.31 | 0.32 | 0.17 | 0.17 | 0.17 | 0.17 |

Calculated melts produced by 1%, 2%, and 3% batch partial melting are no. 1 to no. 18, and no. 19 is the measured, average concentration of the Euphrates lavas. The starting mode, melt mode and mantle source type used to produce each of the calculated melts are as follows:
Melt no. 1–3; starting mode a, melt mode a, mixed source, for 1, 2, and 3% melting, respectively,
no. 4–6; starting mode b, melt mode b, mixed source, for 1, 2, and 3% melting, respectively,
no. 7–9; starting mode c, melt mode c, mixed source, for 1, 2, and 3% melting, respectively,
Melt no. 10–12; starting mode a, melt mode a, primitive source, for 1, 2, and 3% melting, respectively,
no. 13–15; starting mode b, melt mode b, primitive source, for 1, 2, and 3% melting, respectively,
no. 16–18; starting mode c, melt mode c, primitive source, for 3, 2, and 1% melting, respectively.
The composition of the calculated melt no. 18 (produced by 1% melting of garnet lherzolite of a primitive mantle source) closely matches that of the measured average composition of the Euphrates lavas (no. 19). See text for details.

Table 6. Model parameters, mineralogical composition of source rocks and eutectic liquid, chemical composition of the metasomatized source rock used, and results of partial melting calculations for the Euphrates volcanic field of northeastern Syria

| | | Source rocks | | | | Eutectic liquid | | | | |
|---|---|---|---|---|---|---|---|---|---|---|
| Phase | | Gt–Lhr | Gt–Sp–Lhr | Sp–Lhr | | Gt–Lhr | Gt–Sp–Lhr | Sp–Lhr | | |
| Olivine | | 60.1 | 58.5 | 57.0 | | 0.78 | 2.0 | 1.21 | | |
| Opx | | 18.9 | 22.1 | 25.5 | | 5.22 | 8.0 | 8.06 | | |
| Cpx | | 13.7 | 14.1 | 15.0 | | 47.0 | 50.0 | 76.37 | | |
| Garnet | | 7.3 | 4.3 | 0.0 | | 47.0 | 35.0 | 0.0 | | |
| Spinel | | 0.0 | 1.0 | 2.5 | | 0.0 | 5.0 | 14.36 | | |
| REE | DS1 | MDS | DM5 | 10% | 5% | 4% | 3% | 2% | 1% | Euphr. |
| La | 0.206 | 15.2 | 0.96 | 9.12 | 16.8 | 20.3 | 25.5 | 34.3 | 52.3 | 33.0 |
| Ce | 0.722 | 35.1 | 2.48 | 22.5 | 39.3 | 46.3 | 56.2 | 71.4 | 98.1 | 68.4 |
| Pr | 0.143 | 4.70 | 0.38 | 0.25 | 5.32 | 6.09 | 7.13 | 8.60 | 10.8 | 8.22 |
| Nd | 0.815 | 19.7 | 1.80 | 14.6 | 22.5 | 25.2 | 28.7 | 33.2 | 39.5 | 35.0 |
| Sm | 0.299 | 5.15 | 0.56 | 4.23 | 5.60 | 6.54 | 7.20 | 7.80 | 9.00 | 7.45 |
| Eu | 0.115 | 1.58 | 0.19 | 1.39 | 1.86 | 1.99 | 2.15 | 2.33 | 2.54 | 2.66 |
| Gd | 0.419 | 4.96 | 0.67 | 4.64 | 5.92 | 6.27 | 6.66 | 7.11 | 7.61 | 6.24 |
| Tb | 0.077 | 0.74 | 0.11 | 0.751 | 0.900 | 0.936 | 0.977 | 1.02 | 1.07 | 0.94 |
| Dy | 0.525 | 4.05 | 0.73 | 4.48 | 5.02 | 5.14 | 5.27 | 5.41 | 5.55 | 4.40 |
| Ho | 0.120 | 0.75 | 0.16 | 0.905 | 0.942 | 0.949 | 0.957 | 0.965 | 0.973 | 0.74 |
| Er | 0.347 | 1.80 | 0.44 | 2.36 | 2.31 | 2.296 | 2.29 | 2.28 | 2.27 | 1.79 |
| Tm | 0.054 | 0.204 | 0.064 | 0.301 | 0.267 | 0.261 | 0.255 | 0.250 | 0.245 | 0.21 |
| Yb | 0.347 | 1.03 | 0.40 | 1.66 | 1.37 | 1.32 | 1.28 | 1.24 | 1.20 | 1.21 |
| Lu | 0.054 | 0.122 | 0.060 | 0.214 | 0.164 | 0.157 | 0.150 | 0.144 | 0.138 | 0.167 |

Source rocks Gt–Lhr, Gt–Sp–Lhr, and Sp–Lhr represent garnet lherzolite, garnet–spinel lherzolite and spinel lherzolite, respectively. DS1 shows the chemical composition of the garnet-bearing depleted source, MDS shows the chemical composition of fluids produced by 0.5% fusion of the depleted source, and DM5 shows the chemical composition of the garnet-bearing depleted mantle source with 5% addition of metasomatizing fluids derived from a similar depleted source by 0.5% fusion. The calculated melts listed here and shown in Figure 9 are produced by 10% to 1% partial melting of this metasomatized garnet-bearing depleted source. The average composition of the Euphrates lavas (Euphr.) closely resembles that of the calculated liquid produced by 2% partial melting of the metasomatized garnet-bearing depleted mantle source (see text for details).

the various modelling calculations made, a match was produced as a result of a small degree of partial melting (2 % melting; Fig. 9) of a garnet-bearing depleted source (garnet peridotite) enriched with 5 % addition of metasomatizing fluids derived from a similar depleted source by 0.5 % melting.

However, the overall chemical and petrological characteristics are more consistent with the generation of the Euphrates magma by a small degree of partial melting (F = 1 %) of a fertile, garnet-lherzolite, asthenospheric mantle source (cf. Fig. 8), possibly containing a minor spinel component.

### 6.d. The geodynamic framework

The Euphrates volcanic field is located near the Bitlis collision suture, which represents a major plate boundary (cf. Fig. 2). This tectonic feature was created by, and is continuously being reshaped as a result of, movements of both the African and the Arabian plates with respect to the Eurasian plate. The lithospheric mantle of the northern border of the Arabian plate was deformed during and after the collision which led to the formation of the Bitlis suture (current tectonic regime). This could have provoked the development of shear zones; the equivalent at great depth of detached or transform faults observed in the underlying continental base. According to Spera (1987), the rise of magmas by such a network of deformation and fractures could explain the extrusion to the surface (the eruption) of alkaline magmas. Chemical characteristics of the Plio-Quaternary Euphrates lavas reflect their within-plate nature, consistent with magma generation in an extensional tectonic regime.

As indicated above, the Euphrates graben/fault system was developed by extension/transtension following a period of extensive uplift and erosion during the Jurassic and Early Cretaceous (Brew *et al.* 2001). This graben is considered to represent manifestation of re-activated pre-Cenozoic structures that responded to forces acting along nearby Arabian plate boundaries (Cenozoic collision along the Bitlis suture: Sawaf *et al.* 1993). The graben becomes more pronounced in the complex region where it intersects the NE-trending Palmyride mountain belt northwest of Der Azzour. Based on seismic reflection data, Sawaf *et al.* (1993) showed that Quaternary volcanism produced basaltic flows (including the Euphrates volcanic field) above some of the deeper penetrating faults (Palmyride trend) and along a northwestern (Euphrates) fault system where it cuts the western side of the Derro high, also indicating a deeply penetrating fault.

Sawaf *et al.* (1993) also demonstrated that a slight crustal thinning, from 37 km south and north of the Euphrates depression to 35 km beneath it, can account for the subtle change in the long-wavelength Bouguer gravity anomaly over it. The geophysical study of Brew *et al.* (1997) showed that basement depth on the north

https://doi.org/10.1017/S0016756808004901 Published online by Cambridge University Press

side of the Euphrates is about 6 km, while south of it the basement depth is at least 8.5 km, and those authors interpreted this difference in basement depth on adjacent sides of the graben system as an indication that the Euphrates system is a suture/shear zone. This suture may represent a zone of weakness between distinct crustal blocks, possibly inherited from Late Proterozoic accretion of the Arabian plate. Thus, the nature of the Euphrates volcanic rocks, combined with the regional geological context and the overall tectonic framework, suggest that volcanism has occurred in a localized tensional regime.

In their study of volcanism in East Anatolia, Pearce *et al.* (1990) indicated that perturbation of the thickened lithosphere by delamination of the thermal boundary layer, perhaps coupled with local stretching associated with pull-apart basins on strike-slip fault systems, is sufficient to generate melt. Litak *et al.* (1997) demonstrated that Neogene continental collision along the northern and eastern Arabian plate boundaries caused minor reactivation of the Euphrates fault system, in harmony with significant inversion and the main phase of uplift of the nearby Palmyride and Sinjar mountains. In their study of the Neogene volcanic activity of western Syria, Lustrino & Sharkov (2006) proposed that the transition from strongly compressive to transtensional stresses may have allowed for partial melting as a consequence of mantle decompression. In the Euphrates region, heat necessary for magma generation may have been the result of adiabatic decompression and melting. Reactivation of deep-seated fractures beneath the Euphrates graben was interpreted to have resulted as a consequence of Neogene collision of the Arabian plate with Eurasia along the Bitlis suture (Litak *et al.* 1997). The lavas may have penetrated the crust along such reactivated fractures beneath the Euphrates basin.

## 7. Conclusions

(1) The Plio-Quaternary Euphrates volcanic field of northeastern Syria occurs along the northern extension of the Palmyride zone at its intersection with the Euphrates graben. This volcanic field represents the northern segment of the Cenozoic volcanic province of the Middle East and is located near the collision (Bitlis) suture of the Arabian and the Eurasian plates. The lavas form relatively thick discontinuous successions. They are mostly phyric, consisting of about 45–55 vol. % plagioclase, 30–35 % clinopyroxene, 15–20 % olivine and opaque phases.

(2) Rocks of the Euphrates volcanic field are mostly basanites and alkali basalts, have a narrow range of major element compositions ($SiO_2$, 38.2–45.5 wt %; MgO, 8.7–13.0 wt %), are alkaline in nature, and are enriched in Ti (2.5–3.5 wt % $TiO_2$), Zr (133–276 ppm), Nb (25–71 ppm) and Y (17–28 ppm). The primitive mantle-normalized patterns are strongly fractionated ($(La/Yb)_N = 19.6$) and conformable. The $^{143}Nd/^{144}Nd$ isotopic composition of the Euphrates lavas ranges from 0.512868 to 0.512940 and $^{87}Sr/^{86}Sr$ from 0.70309 to 0.70352. The overall chemical and isotopic compositions of these lavas reflect strong affinities to OIB. The relatively uniform $^{143}Nd/^{144}Nd$ ($\varepsilon_{Nd} = 4.5$ to 5.9) for the Euphrates volcanic field suggests that its magma was developed by partial melting of an isotopically uniform mantle source.

(3) Elemental ratios such as K/P (3.4, on average), La/Ta (13) and La/Nb (0.77), and the very low silica values (43.1 wt % $SiO_2$), suggest that crustal contamination did not play a significant role during magma evolution; the magmas probably experienced very rapid ascent.

(4) Petrogenetic modelling suggests that the magma could have been produced as a result of a small degree of partial melting of either (1) a garnet-bearing depleted source enriched with a small addition of metasomatizing fluids, or (2) a garnet-bearing fertile source. The overall chemical and petrological characteristics are more consistent with the generation of the Euphrates magma by a small degree of partial melting (F = 1 %) of a primitive, garnet-lherzolite mantle source, possibly containing a minor spinel component. The Euphrates volcanic field displays the geochemical characteristics of within-plate lavas. Heat necessary for magma generation may have been the result of adiabatic decompression and melting. The Neogene collision of the Arabian plate with Eurasia along the Bitlis suture resulted in reactivation (beneath the Euphrates basin) of deep-seated fractures, along which lavas may have penetrated the crust.

**Acknowledgements.** We would like to note that the collaboration of Roger Laurent (Laval University, Québec) was essential in this study. We thank Alan Dickin at MacMaster University, Ontario, for isotope analysis work. We appreciate the help of A. A. Turkmani, Ministry of Petroleum and Mineral Resources, Syria, during the field work, as well as that from Muawia Barazangi and Graham Brew at Cornell University and Michel Delaloye of the University of Geneva. We acknowledge the technical support provided by M. Ijreiss of the American University of Beirut (Lebanon). This work was part of a larger research project made possible by grants from the Fonds pour la formation de chercheurs et l'aide à la recherche (Québec) and the Conseil de recherches en sciences humaines du Canada. Valuable comments made by the two referees (J. Baker and T. Furman) improved our contribution.

## References

ABDEL-RAHMAN, A. M. 2002. Mesozoic volcanism in the Middle East: geochemical, isotopic and petrogenetic evolution of extension-related alkali basalts from central Lebanon. *Geological Magazine* **139**, 621–40.

https://doi.org/10.1017/S0016756808004901 Published online by Cambridge University Press

ABDEL-RAHMAN, A. M. & KUMARAPELI, P. S. 1999. Geochemistry and petrogenesis of the Tibbit Hill metavolcanic suite of the Appalachian Fold Belt, Quebec–Vermont: a plume-related and fractionated assemblage. *American Journal of Science* **299**, 210–37.

ABDEL-RAHMAN, A. M. & NASSAR, P. E. 2004. Cenozoic volcanism in the Middle East: petrogenesis of alkali basalts from northern Lebanon. *Geological Magazine* **141**, 545–63.

ALLÈGRE, C. J., HAMELIN, B., PROVOST, A. & DUPRÉ, B. 1987. Topology in isotopic multispace and origin of mantle chemical heterogeneities. *Earth and Planetary Science Letters* **81**, 319–37.

ALLÈGRE, C. J. & MINSTER, J. F. 1978. Quantitative models of trace element behavior in magmatic processes. *Earth and Planetary Science Letters* **38**, 1–25.

BAKER, J. A., CHAZOT, G., MENZIES, M. A. & THIRLWALL, M. F. 1998. Metasomatism of the shallow mantle beneath Yemen by the Afar plume – Implications for mantle plumes, flood volcanism, and intraplate volcanism. *Geology* **26**, 431–4.

BAKER, J. A., MENZIES, M. A., THIRLWALL, M. F. & MACPHERSON, C. J. 1997. Petrogenesis of Quaternary intraplate volcanism, Sana'a, Yemen: implications for plume–lithosphere interaction and polybaric melt hybridization. *Journal of Petrology* **38**, 1359–90.

BAKER, J. A., THIRLWALL, M. F. & MENZIES, M. A. 1996. Sr–Nd–Pb isotopic and trace element evidence for crustal contamination of plume-derived flood basalts: Oligocene flood volcanism in western Yemen. *Geochimica et Cosmochimica Acta* **60**, 2559–81.

BALDRIDGE, W. S., EYAL, Y., BARTOV, Y., STEINITZ, G. & EYAL, M. 1991. Miocene magmatism of Sinai related to the opening of the Red Sea. *Tectonophysics* **197**, 181–201.

BARBERI, F., FERRARA, G., SANTACROCE, R., TREUIL, M. & VARET, J. 1975. A transitional basalt–pantellerite sequence of fractional crystallization: The Boina center (Afar rift, Ethiopia). *Journal of Petrology* **16**, 22–56.

BARRAT, J. A., FOURCADE, S., JAHN, B. M., CHEMINÈE, J. L. & CAPDEVILA, R. 1998. Isotope (Sr, Nd, Pb, O) and trace element geochemistry of volcanics from the Erta' Ale range (Ethiopia). *Journal of Volcanology and Geothermal Research* **80**, 85–100.

BERTRAND, H., CHAZOT, G., BLICHERT-TOFT, J. & THORAL, S. 2003. Implications of widespread high-m volcanism on the Arabian Plate for Afar mantle plume and lithosphere composition. *Chemical Geology* **198**, 47–61.

BRADSHAW, T. K. & SMITH, E. I. 1994. Polygenetic Quaternary volcanism at Crater Flat, Nevada. *Journal of Volcanology and Geothermal Research* **63**, 165–82.

BREW, G. E., BARAZANGI, M., AL-MALEH, A. K. & SAWAF, T. 2001. Tectonic and geologic evolution of Syria. *GeoArabia* **6**, 573–615.

BREW, G. E., LITAK, R. K., SEBER, D., BARAZANGI, M., AL-IMAN, A. & SAWAF, T. 1997. Basement depth and sedimentary velocity structure in the northern Arabian platform, eastern Syria. *Geophysical Journal International* **128**, 617–31.

CAMP, V. E. & ROOBOL, M. J. 1989. The Arabian continental alkali basalt province: Part I. Evolution of Harrat Rahat, Kingdom of Saudia Arabia. *Geological Society of America Bulletin* **101**, 71–95.

CAMP, V. E. & ROOBOL, M. J. 1992. Upwelling asthenosphere beneath western Arabia and its regional implications. *Journal of Geophysical Research* **97B**, 15255–71.

CAMP, V. E., ROOBOL, M. J. & HOOPER, P. R. 1992. The Arabian continental alkali basalt province: Part III. Evolution of Harrat Kishb, Kingdom of Saudia Arabia. *Geological Society of America Bulletin* **104**, 379–96.

CHAFFEY, D. J., CLIFF, R. A. & WILSON, B. M. 1989. Characterization of the St Helena magma sourse. In *Magmatism in the ocean basins* (eds A. D. Saunders & M. J. Norry), pp. 257–76. Geological Society of London, Special Publication no. 42.

CHEN, W. & ARCULUS, R. J. 1995. Geochemical and isotopic characteristics of lower crustal xenoliths, San Francisco Volcanic Field, Arizona, U.S.A. *Lithos* **36**, 203–25.

DUBERTRET, L. 1955. *Carte Geologique du, Liban aux 1/200,000, avec notice explicative*. Beyrouth: Ministire des Travaux Public, 74 pp.

EBINGER, C. J. & SLEEP, N. H. 1998. Cenozoic magmatism throughout east Africa resulting from impact of a single plume. *Nature* **395**, 788–91.

ELLAM, R. M. 1992. Lithospheric thickness as a control on basalt geochemistry. *Geology* **20**, 153–6.

FITTON, J. G., JAMES, D. & LEEMAN, W. P. 1991. Basic magmatism associated with Late Cenozoic extension in the western United States: compositional variations in space and time. *Journal of Geophysical Research* **96**, 13693–712.

FREY, F. A., CLAGUE, D., MAHONEY, J. J. & SINTON, J. M. 2000. Volcanism at the edge of the Hawaiian plume: petrogenesis of submarine alkalic lavas from the North Arch Volcanic Field. *Journal of Petrology* **41**, 667–91.

FREY, F. A., GARCIA, M. O., WISE, W. S., KENNEDY, A., GURRIET, P. & ALBAREDE, F. 1991. The evolution of Mauna Kea volcano, Hawaii: Petrogenesis of tholeiitic and alkali basalts. *Journal of Geophysical Research* **96**, 14347–75.

FURMAN, T., BRYCE, J. G., KARSON, J. & IOTTI, A. 2004. East African Rift System (EARS) plume structure: insights from Quaternary mafic lavas of Turkana, Kenya. *Journal of Petrology* **45**, 1069–88.

FURMAN, T., KALETA, K. M., BRYCE, J. G. & HANAN, B. B. 2006. Tertiary mafic lavas of Turkana, Kenya: constraints on East African plume structure and the occurrence of high–$\mu$ volcanism in Africa. *Journal of Petrology* **47**, 1221–44.

GARFUNKEL, Z. 1989. Tectonic Setting of Phanerozoic magmatism in Israel. *Israel Journal of Earth Sciences* **38**, 51–74.

GEORGE, R. & ROGERS, N. 2002. Plume dynamics beneath the African plate inferred from the geochemistry of the Tertiary basalts of southern Ethiopia. *Contributions to Mineralogy and Petrology* **144**, 286–304.

GIANNÉRINI, G., CAMPREDON, R., FÉRAUD, G. & Abou ZAKHEM, B. 1988. Déformations intraplaques et volcanisme associé: exemple de la bordure NW de la plaque Arabique au Cénozoïque. *Bulletin de la Société Géologique de France* **8**(6), 937–47.

GIBB, F. G. F. & HENDERSON, C. M. B. 2006. Chemistry of the Shiant Isles main sill, NW Scotland, and wider implications for the petrogenesis of mafic sills. *Journal of Petrology* **47**, 191–230.

GIBSON, S. A., THOMPSON, R. N., DICKIN, A. P. & LEONARDOS, O. H. 1995. High-Ti and low-Ti mafic potassic magmas: key to plume–lithosphere interactions and continental flood-basalt genesis. *Earth and Planetary Science Letters* **136**, 149–65.

GIBSON, S. A., THOMPSON, R. N., WESKA, R. K., DICKIN, A. P. & LEONARDOS, O. H. 1997. Late Cretaceous rift-related upwelling and melting of the Trinidade starting mantle plume head beneath western Brazil. *Contributions to Mineralogy and Petrology* **126**, 303–14.

HANSON, G. N. 1980. Rare earth elements in petrogenetic studies of igneous systems. *Annual Reviews in Earth Sciences* **8**, 371–406.

HART, S. R. 1988. Heterogeneous mantle domains: signatures, genesis and mixing chronologies. *Earth and Planetary Science Letters* **90**, 273–96.

HART, W. K., WOLDE, G. C., WALTER, R. C. & MERTZMAN, S. A. 1989. Basaltic volcanism in Ethiopia: constraints on continental rifting and mantle interactions. *Journal of Geophysical Research* **94**, 7731–48.

HOFMANN, A. W. 1997. Mantle geochemistry: the message from oceanic volcanism. *Nature* **385**, 219–29.

LASSITER, J. C., DEPAOLO, D. J. & MAHONEY, J. J. 1995. Geochemistry of the Wrangellia Flood Basalt Province: implications for the role of continental and oceanic lithosphere in flood basalt genesis. *Journal of Petrology* **36**, 983–1009.

LAWS, E. D. & WILSON, M. 1997. Tectonics and magmatism associated with Mesozoic passive continental margin development in the Middle East. *Journal of the Geological Society, London* **154**, 757–60.

LE BAS, M. J. & STRECKEISEN, A. L. 1991. The IUGS systematics of igneous rocks. *Journal of the Geological Society of London* **148**, 825–33.

LITAK, R. K., BARAZANGI, M., BEAUCHAMP, W., SEBER, D., BREW, G., SAWAF, T. & AL-YOUSSEF, W. 1997. Mesozoic–Cenozoic evolution of the intraplate Euphrates fault system, Syria: implications for regional tectonics. *Journal of the Geological Society of London* **154**, 653–66.

LUSTRINO, M. & SHARKOV, E. 2006. Neogene volcanic activity of western Syria and its relationship with Arabian plate kinematics. *Journal of Geodynamics* **42**, 140–58.

LYBERIS, N., YURUR, T., CHOROWICZ, J., KASAPOGLU, E. & GUNDOGDU, N. 1992. The East Anatolian Fault: an oblique collisional belt. In *The Afro-Arabian Rift System* (ed. R. Altherr), pp. 1–15. *Tectonophysics* **204**.

MCKENZIE, D. P. & O'NIONS, R. K. 1991. Partial melting distributions from inversion of rare earth element concentrations. *Journal of Petrology* **32**, 1021–91.

MELLUSO, L., BECCALUVA, L., BROTZU, P., GREGNANIN, A., GUPTA, A. K., MORBIDELLI, L. & TRAVERSA, G. 1995. Constraints on the mantle sources of the Deccan Traps from the petrology and geochemistry of the basalts of Gujarat State (Western India). *Journal of Petrology* **36**, 1393–1432.

MENZIES, M. A. & KYLE, R. 1990. Continental volcanism: a crust–mantle probe. In *Continental Mantle* (ed. M. A. Menzies), pp. 157–77. Oxford: Oxford Science Publishers.

MOHR, P. 1983. Ethiopian flood basalt province. *Nature* **303**, 577–84.

MOUTY, M., DELALOYE, M., FONTIGNIE, D., PISKIN, O. & WAGNER, J.-J. 1992. The volcanic activity in Syria and Lebanon between Jurassic and actual. *Schweizerische Mineralogische und Petrografische Mitteilungen* **72**, 91–105.

NOTSU, K., FUJITANI, T., UI, T., MATSUDA, J. & ERCAN, T. 1995. Geochemical features of collision-related volcanic rocks in central and eastern Anatolia, Turkey. *Journal of Volcanology and Geothermal Research* **64**, 171–92.

PEARCE, J. A. 1983. Role of the sub-continental lithosphere in magma genesis at active continental margins. In *Continental basalts and mantle xenoliths* (eds C. J. Hawkesworth & M. J. Norry), pp. 230–49. Cheshire, U.K.: Shiva.

PEARCE, J. A., BENDER, J. F., DE LONG, S. E., KIDD, W. S. F., LOW, P. J., GÜNER, Y., SAROĞLU, F., YILMAZ, Y., MOORBATH, S. & MITCHELL, J. G. 1990. Genesis of collision volcanism in Eastern Anatolia, Turkey. *Journal of Volcanology and Geothermal Research* **44**, 189–229.

PIK, R., DENIEL, C., COULON, C., YIRGU, G. & MARTY, B. 1999. Isotopic and trace element signatures of Ethiopian flood basalts; evidence for plume–lithosphere interactions. *Geochimica et Cosmochimica Acta* **63**, 2263–79.

PONIKAROV, V. P. (EDITOR-IN-CHIEF) 1967. *The Geology of Syria: Explanatory Notes on the Geological Map of Syria, Scale 1:5 000 000, Part I, Stratigraphy, Igneous Rocks and Tectonics*. Damascus, Syria: Ministry of Industry, 88 pp.

RICHARD, P., SHIMIZU, N. & ALLÈGRE, C. J. 1976. $^{143}Nd/^{144}Nd$, a natural tracer: an application to oceanic basalts. *Earth and Planetary Science Letters* **31**, 269–78.

SAWAF, T., AL-SAAD, D., GEBRAN, A., BARAZANGI, M., BEST, J. A. & CHAIMOV, T. 1993. Stratigraphy and structure of eastern Syria across the Euphrates depression. *Tectonophysics* **220**, 267–81.

SHAW, D. M. 1970. Trace element fractionation during anatexis. *Geochimica et Cosmochimica Acta* **34**, 237–43.

SHAW, J. E., BAKER, J. A., MENZIES, M. A., THIRLWALL, M. F. & IBRAHIM, K. M. 2003. Petrogenesis of the largest intraplate volcanic field on the Arabian Plate (Jordan): a mixed lithosphere–asthenosphere source activated by lithospheric extension. *Journal of Petrology* **44**, 1657–79.

SMITH, E. I., SÁNCHEZ, A., WALKER, J. D. & WANG, K. 1999. Geochemistry of mafic magmas in the Hurricane Volcanic Field, Utah: implications for small- and large-scale chemical variability of the lithospheric mantle. *Journal of Geology* **107**, 433–48.

SPERA, F. J. 1987. Dynamics of translithospheric migration of metasomatic fluid and alkaline magma. In *Mantle metasomatism* (eds M. A. Menzies & C. J. Hawkesworth), pp. 11–20. London: Academic Press.

STAUDIGEL, H., ZINDLER, A., HART, S. R., LESLIE, C. Y. & CLAGUE, D. 1984. The isotope systematics of a juvenile intra-plate volcano: Pb, Nd and Sr isotope ratios of basalts from Loihi Seamount, Hawaii. *Earth and Planetary Science Letters* **69**, 13–29.

STEWART, K. & ROGERS, N. 1996. Mantle plume and lithosphere contributions to basalts from southern Ethiopia. *Earth and Planetary Science Letters* **139**, 195–211.

SUN, S. & MCDONOUGH, W. F. 1989. Chemical and isotopic systematics of oceanic basalts: implications for mantle composition and processes. In *Magmatism in the ocean basins* (eds A. D. Saunders & M. J. Norry), pp. 313–45. Geological Society of London, Special Publication no. 42.

VOLKER, F., ALTHERR, R., JOCHUM, K.-P. & MCCULLOCH, M. T. 1997. Quaternary volcanic activity of the southern Red Sea: new data and assessment of models on magma sources and Afar plume-lithosphere interaction. *Tectonophysics* **278**, 15–29.

WEAVER, B. L. 1991. Trace element evidence for the origin of ocean-island basalts. *Geology* **19**, 123–6.

WEINSTEIN, Y., NAVON, O., ALTHERR, R. & STEIN, M. 2006. The role of lithospheric mantle heterogeneity in the generation of Plio-Pleistocene alkali basaltic suites from

Harrat Ash Shaam (Israel). *Journal of Petrology* **47**, 1017–50.

WHITE, W. M. 1985. Sources of oceanic basalts: radiogenic isotopic evidence. *Geology* **13**, 115–18.

WHITE, R. S. & MCKENZIE, D. P. 1989. Magmatism at rift zones: the generation of volcanic continental margins and flood basalts. *Journal of Geophysical Research* **94**, 7685–730.

WILSON, M. 1993. Geochemical signatures of oceanic and continental basalts: a key to mantle dynamics? *Journal of the Geological Society, London* **150**, 977–90.

WITT-EICKSCHEN, G. & KRAMM, U. 1997. Mantle upwelling and metasomatism beneath central Europe: geochemical and isotopic constraints from mantle xenoliths from the Rhon (Germany). *Journal of Petrology* **38**, 479–93.

https://doi.org/10.1017/S0016756808004901 Published online by Cambridge University Press